JPET Fast Forward. Published on November 10, 2020 as DOI: 10.1124/jpet.120.000309
This article has not been copyedited and formatted. The final version may differ from this version.

Lysosomal Biogenesis and Implications for Hydroxychloroquine Disposition

Keagan P Collins, Sandra Witta, Jonathan W Coy, Yi Pang, Daniel L Gustafson

Colorado State University

Affiliations:

School of Biomedical Engineering; Colorado State University; Fort Collins, CO USA (KPC, SW, DLG); Department of Clinical Sciences; Colorado State University; Fort Collins, CO USA (DLG, JWC); University of Colorado Cancer Center; Anschutz Medical Campus; Aurora, CO USA (DLG); University of Akron; Department of Chemistry; Akron, OH USA (YP)

JPET Fast Forward. Published on November 10, 2020 as DOI: 10.1124/jpet.120.000309
This article has not been copyedited and formatted. The final version may differ from this version.

Corresponding Author:

Daniel L Gustafson, Ph.D.

Flint Animal Cancer Center

300 West Drake Road, FACC246

Fort Collins, CO 80523

daniel.gustafson@colostate.edu

Running Title: Lysosomal Biogenesis and Hydroxychloroquine Disposition

Text Pages: 27

Tables: 3

Figures: 6

References: 36

Abstract: 216

Introduction: 747

Discussion: 964

Keywords: hydroxychloroquine, pharmacokinetic model, TFEB, lysosome

Abbreviations: area under the curve (AUC), chloroquine (CQ), drug-drug interaction (DDI), hydroxychloroquine (HCQ), median absolute performance error (MAPE), multiple drug resistant (MDR), Monensin (MN), median performance error (MPE), performance error (PE), pharmacokinetic (PK), Torin1 (T1), transcription factor EB (TFEB)

Recommended Section Assignment: Chemotherapy, Antibiotics, and Gene Therapy

JPET Fast Forward. Published on November 10, 2020 as DOI: 10.1124/jpet.120.000309
This article has not been copyedited and formatted. The final version may differ from this version.

Abstract

Lysosomes act as a cellular drug sink for weakly basic, lipophilic (lysosomotropic) xenobiotics, with many instances of lysosomal trapping associated with MDR. Lysosomotropic agents have also been shown to activate master lysosomal biogenesis transcription factor EB (TFEB), and ultimately lysosomal biogenesis. We investigated the role of lysosomal biogenesis in the disposition of hydroxychloroquine (HCQ), a hallmark lysosomotropic agent, and observed that modulating the lysosomal volume of human breast cancer cell lines can account for differences in disposition of HCQ. Through use of an *in vitro* pharmacokinetic (PK) model we characterized total cellular uptake of HCQ within the duration of static equilibrium (1 hour), as well as extended exposure to HCQ that are subject to dynamic equilibrium (>1 hour) wherein HCQ increases the size of the lysosomal compartment through swelling and TFEB-induced lysosomal biogenesis. In addition, we observe that pretreatment of cell lines with TFEB-activating agent Torin 1 contributed to an increase of whole cell HCQ concentrations by 1.4 to 1.6-fold, which were also characterized by the *in vitro* PK model. This investigation into the role of lysosomal volume dynamics in lysosomotropic drug disposition, including the ability of HCQ to modify its own disposition, advances our understanding of how chemically-similar agents may distribute on the cellular level, and examines a key area of lysosomal-mediated MDR and DDI.

Significance Statement

Hydroxychloroquine is able to modulate its own cellular pharmacokinetic uptake by increasing the cellular lysosomal volume fraction through activation of lysosomal biogenesis master transcription factor EB, and through lysosomal swelling. This concept can be applied to many other lysosomotropic drugs that activate TFEB, such as doxorubicin and other TKI drugs, where these drugs may actively increase their own sequestration within the lysosome to further exacerbate MDR and lead to potential acquired resistance.

JPET Fast Forward. Published on November 10, 2020 as DOI: 10.1124/jpet.120.000309
This article has not been copyedited and formatted. The final version may differ from this version.

Introduction

Hydroxychloroquine (HCQ) has been investigated in over 50 cancer clinical trials and countless preclinical studies through the past decade as an additive compound to primary chemotherapy treatment. Mechanistically, HCQ acts to inhibit autophagy, which has been identified as a mechanism of tumor cell resistance to chemotherapy and a key pathway to survival within the tumor microenvironment. While next generation autophagy inhibitors are in preclinical stages of development, HCQ remains the only clinically approved autophagy inhibitor. Overall HCQ is generally effective and safe as a treatment but suffers from various pitfalls within the pharmacologic space – specifically in terms of predictability of patient likelihood of response and reliable pharmacokinetic (PK) and pharmacodynamic (PD) metrics. There is a general disconnect between HCQ PK in the tumor and blood; creating a challenge when optimizing dosing strategies to be confident that target concentrations of HCQ are achieved within the tumor (Barnard et al., 2014). Characterization of HCQ PK properties on a cellular level may provide insight towards tumor-specific factors that would promote this disconnect.

Cellular uptake of HCQ is driven primarily through lysosomal ion-trapping due to its weakly basic and lipophilic properties that characterize it as a hallmark lysosomotropic agent. HCQ readily diffuses through neutral spaces, but becomes diprotonated in the lysosome, whose acidic environment facilitates accumulation. This results in concentrations significantly higher than other compartments within the cell (Duvvuri and Krise, 2005). Key mechanisms contributing to pharmacokinetics have been considered and consolidated into *in vitro* mathematical models to describe cellular uptake of compounds with similar physicochemical properties to HCQ, namely weakly basic and lipophilic (Ishizaki et al., 2000; Trapp et al., 2008; Kornhuber et al., 2010; Schmitt et al., 2019). These models assume the cell behaves as a static

JPET Fast Forward. Published on November 10, 2020 as DOI: 10.1124/jpet.120.000309
This article has not been copyedited and formatted. The final version may differ from this version.

system of compartments, but recent evidence suggests that lysosomotropic compounds induce changes in the lysosome itself.

Lysosomes swell in response to chloroquine (CQ) exposure, which is mechanistically and pharmacokinetically similar to HCQ. Near clinically-relevant doses of CQ have been observed to cause a 3-fold increase in relative lysosomal volume after multiple days of exposure to the drug (King et al., 2016), and recruitment of galectin-3 to sites on these swollen lysosomes, indicating membrane damage (Gallagher et al., 2017). In addition to an increase in lysosomal size, an increase in lysosomal number has also been reported in response to a panel of lysosomotropic agents, including CQ, over the course of 4 and 24 hours (Lu et al., 2017). This increase in lysosomal number was linked to an increase in nuclear translocation of master lysosomal biogenesis transcription factors, TFEB, TFE3, and MITF. TFEB activation of the CLEAR network of genes has been described as the master regulation system of lysosomal biogenesis (Settembre et al., 2012; Settembre et al., 2013). Lysosomotropic agents cause activation of this network by inducing lysosomal stress, and has been shown to activate as early as 90 minutes of exposure to CQ (Zhitomirsky et al., 2018). The results of lysosomal swelling and TFEB activation by lysosomotropic agents may be linked to their long-term tissue PK. Extended dosing of HCQ is characterized by a consistent increase in HCQ concentrations in rat tissue over the course of 3 months of daily dosing. In some tissues (spleen, kidney, liver, heart) HCQ concentrations continued to increase out to the latest timepoint measured at 7 months (McChesney, 1983). This long-term PK profile is noted by McChesney to be similar to other lysosomotropic drugs such as chlorpromazine.

Due to the frequent, high doses of HCQ used in cancer clinical trials we characterized this lysosomal adaptation response on a cellular level and investigated the extent to which it may influence cellular disposition of the drug. The data described herein suggests that baseline cell uptake of HCQ is associated with different baseline lysosomal profiles between cell lines,

JPET Fast Forward. Published on November 10, 2020 as DOI: 10.1124/jpet.120.000309
This article has not been copyedited and formatted. The final version may differ from this version.

which were integrated into a lysosome cellular PK mathematical model (Trapp et al., 2008; Kornhuber et al., 2010) to accurately model whole cell HCQ PK to chemical kinetic equilibrium. Small, but consistent increases in whole cell uptake of HCQ over an extended time period were also observed, and attributed to an increasing volume of the lysosomal compartment. The *in vitro* PK profile of HCQ was thus broken up into a short-term kinetic equilibrium portion, within 1 hour of exposure, and a long-term dynamic portion, out to 24 hours of exposure for all cell lines. This data was used, in conjunction with observed differences in baseline lysosomal profiles, to further characterize the cellular PK of HCQ by accounting for a dynamic lysosomal compartment.

Materials and Methods

Cell Lines

Human breast cancer cell lines including MDA-MB-231, MDA-MB-468, T47D, and MCF7 human breast cancer cell lines were purchased from Cell Culture Services at University of Colorado Anschutz Medical Campus (Aurora, CO). For cell pharmacokinetic experiments, all cell lines were stably transfected with Incucyte NucLight Red Lentivirus (Sartorius, Cat. 4476) prior to experimentation.

Cell lines were cultured in Dulbecco's Modified Essential Medium (Corning, 10-017-CV) supplemented with 10% fetal bovine serum (Peak Serum, PS-FB3), 1% penicillin/streptomycin (Fisher, 30-002-CI), and 1% sodium pyruvate (Fisher, 25-000-CI) at 37°C and 5% CO2 in a humidified incubator.

Chemicals and Reagents

Hydroxychloroquine (HCQ) sulfate was purchased from SigmaAldrich (St. Louis, MO). Monensin (MN) was purchased from VWR (Radnor, PA). Torin1 (T1) was purchased from Fisher (Hampton, NH). Hoechst 33342 20mM solution (62249) and CellLight Lysosomes-GFP,

JPET Fast Forward. Published on November 10, 2020 as DOI: 10.1124/jpet.120.000309
This article has not been copyedited and formatted. The final version may differ from this version.

BacMam 2.0 (C10507) were purchased from ThermoFisher (Waltham, MA). ETP, a pH-insensitive lysosomal lumen dye applicable for live and fixed cell imaging, was received as a gift from Dr. Yi Pang at the University of Akron (Abeywickrama et al., 2019).

Cell Uptake Experiments

4 human breast cancer cell lines were used to perform experiments. The first 2, MBA-MB-231 and MDA-MB-468, are mechanistically sensitive to autophagy inhibition through gene knockdown (Maycotte et al., 2014; Towers et al., 2019) and pharmacologically sensitive to hydroxychloroquine. The second 2, MCF7 and T47D, are insensitive to both methods (Maycotte et al., 2014).

Cell lines were cultured in standard DMEM supplemented with 10% FBS, 1% PS, and 1% sodium pyruvate in an incubator at 37°C and 5% CO2. T47D and MCF7 cell lines required supplementation of 8μg/mL of insulin to maintain growth. For acidic media experiments with MDA-MB-231 cells, DMEM without sodium bicarbonate was purchased, and bicarbonate was added to achieve an incubator-conditioned media pH. Culture media buffers other than sodium bicarbonate, such as HEPES, were purposely omitted as HEPES has been shown to activate the MiT/TFE network, resulting in lysosomal biogenesis (Tol et al., 2018).

Cell lines were plated, allowed to adhere overnight, and treated at roughly 70% confluence. All cell lines stably expressed NucLight Red, and cell counts were measured by counting red fluorescent nuclei on an Incucyte ZOOM (Sartorius; Gottingen, Germany) prior to treatment with drug. For 4 hour and 24-hour timepoints cells were counted immediately prior to harvesting, as the doubling time for these cell lines is between 16-20 hours. Experiments were not extended past 24 hours to avoid cell line growth inhibition in response to HCQ. For treatment, culture media was aspirated and replaced with fresh, incubator-conditioned media containing 10μM HCQ and placed in a 37° C incubator until the designated timepoint. At the

JPET Fast Forward. Published on November 10, 2020 as DOI: 10.1124/jpet.120.000309
This article has not been copyedited and formatted. The final version may differ from this version.

timepoint cell media containing HCQ was aspirated and cells were washed with HBSS, then trypsinized for 5 minutes. Trypsinized cells were washed off the plate with additional culture media at a ratio of 4:1 media:trypsin. Cells were then pelleted at 1600 rpm for 5 minutes, media was carefully aspirated, and the cell pellet reconstituted in MilliQ-water and frozen until LCMS extraction and analysis.

LC/MS-MS analysis follows methods described in (Barnard et al., 2014), but briefly – cell pellets were vortexed and lysed for 10 minutes in a sonication water bath. Acetonitrile (ACN) was then added to the cell pellets to yield a final solution of 50% ACN + 50% MilliQ-H_2O. Cells were vortexed for 10 minutes, then centrifuged at 13,300 rpm for 10 minutes. Supernatant was transferred to polypropylene inserts. Chloroquine (CQ) was used as an internal standard. Concentrations of supernatant obtained on LC/MS-MS were normalized to the cell counts obtained for each sample from an Incucyte ZOOM, and samples were then normalized to cell volume, obtained for each cell line from suspended cell diameter measured on a Countess system (n=4), to obtain HCQ concentration (μM) in each cell.

For experiments with monensin (MN), cells were pretreated with 25μM MN for 30 minutes prior to adding HCQ. After 30 minutes 10μM HCQ was added for the duration for of the 1hr exposure. For experiments with Torin1 (T1), cells were pretreated with 250nM Torin1 for 16 hours prior to adding HCQ. All cell uptake experiments were performed in at least triplicate.

Lysosomal Imaging

For all imaging experiments cells were plated at 10,000 cells/well on an 8-well glass chamber slide (Cellvis, C8-1.5H-N) and allowed to adhere overnight.

To determine lysosomal volume, live cells were treated with 1μM of ETP (Abeywickrama et al., 2019), and incubated for 30 minutes. Excess dye was removed by washing twice with warm media, and incubated with 10μM of Hoescht 33342 for 10 minutes. Cells were then

JPET Fast Forward. Published on November 10, 2020 as DOI: 10.1124/jpet.120.000309
This article has not been copyedited and formatted. The final version may differ from this version.

washed twice with PBS and fixed for 10 minutes in 2% PFA. PFA was washed off twice with PBS and cells were imaged on an Olympus IX83 microscope with a Plapon 60x Objective, NA = 1.42 on Cy3 and DAPI confocal channels. 43 z-stacks of 0.24μm step-size were captured on Cy3 and DAPI channels. Lysosomal volume fraction of cells was determined using an in-house image processing pipeline which is described briefly as follows: Raw confocal image stacks were converted to .tif files and imported into Python version 3.7.6. A reference image was created by compressing the stack by its maximum pixel intensity. Each slice of each image stack was analyzed to determine the peak signal to noise ratio (PSNR) relative to the reference image using the sewar module (https://pypi.org/project/sewar/). A .csv file containing the top 10 PSNR slices for each image stack was generated and imported into a FIJI macro that calculated the Cy3 (lysosome) area for each raw .vsi image slice based on an algebraic threshold of mean intensity. The area for each slice was multiplied by the step size (0.24μm) to generate a volume, and then volumes from the 10 slices per image stack were summed to generate a lysosomal volume for the image. The lysosomal volume was normalized to the cell count of each image, and the cell count was normalized to the experimentally determined cell volume for each cell line to generate a lysosomal volume fraction per cell. 5-10 images were obtained for each experimental replicate, and lysosomal volume fraction is presented as the mean ± standard deviation of each replicate (n=3) for each cell line. Imaging of cell lines for GFP-LAMP-1 expression followed the same imaging process, except cells were incubated with 1μL of the baculovirus overnight prior to treatment with HCQ.

For drug treated conditions, single plane images were captured at 20x using the same microscope, but an Uplsapo 20x objective, NA = 0.75 on Cy3 and DAPI LED channels. To determine a change in lysosome content of the cell, cells were treated with the same drug treatment conditions as described in the cell uptake experiments section. Chamber slides were prepared in the same way as described above. Images were quantitated using a FIJI macro

JPET Fast Forward. Published on November 10, 2020 as DOI: 10.1124/jpet.120.000309
This article has not been copyedited and formatted. The final version may differ from this version.

with an algebraic threshold of the mean intensity, and data was calculated as Cy3 area / DAPI area. Roughly 10 images were obtained for each experimental replicate, and data is reported as the mean ± standard deviation of each replicate (n=4). Statistical significance was calculated as a one-way ANOVA with Dunnett's multiple comparisons test relative to the control, where $P < 0.05$ was significant.

TFEB Activation

TFEB activation by HCQ was determined with 2 different kinds of methods including gene set enrichment analysis (GSEA) of the TFEB-regulated CLEAR network, and through a TFEB transcription factor activity assay (RayBiotech, TFEH-TFEB). Gene expression microarray data was prepared for all 4 hBC lines following cell culture preparation steps as outlined in the cell uptake experiments section. Cell lines were treated with 20μM HCQ, for 24 hours prior to harvesting for gene expression preparation in triplicate. Prepared cell extraction homogenate was run on an HG_U133_Plus_2 chip. CEL file data was extracted and prepared for GSEA using the Affymetrix Bioconductor package in R, and normalized using RMA. Expression data was then analyzed using the GSEA 4.0.3 software provided by the BROAD Institute. Gene sets from the 4 cell lines, treated with HCQ or vehicle, were analyzed in GSEA using a gene set representative of TFEB lysosome targets (Palmieri et al., 2011) and run in tandem with the Hallmarks of Cancer gene set database version 7.1 provided in the GSEA software. The run was set for 1000 permutations following a "gene_set" permutation type. Data is reported as the NES value and significance determined by FDR q-value generated in the run. Raw .CEL files are available in the supplement. TFEB nuclear activation was performed in duplicate and was determined using the human TFEB transcription factor activity assay following manufacturer's instructions. TFEB activity data is expressed as mean ± standard deviation, and was analyzed by one-way ANOVA with Dunnett's multiple comparison test relative to control with significance as $P < 0.05$.

JPET Fast Forward. Published on November 10, 2020 as DOI: 10.1124/jpet.120.000309
This article has not been copyedited and formatted. The final version may differ from this version.

Cell Pharmacokinetic Mathematical Modeling and Simulation

To connect whole cell HCQ PK with the perturbations observed in the lysosomal compartment, HCQ whole cell uptake was simulated using a previously published base model of lysosomal uptake (Trapp et al., 2008; Kornhuber et al., 2010). Lysosomal volume fraction for each cell line was determined by imaging methods described above. Extracellular pH was determined by measuring the pH of incubator-equilibrated media in a pH meter (7.6), and then testing the change in cellular uptake of HCQ at the 1hr timepoints in a media of decreased pH (7.0). The influence of the lysosome and cytosolic pH were determined experimentally by pretreating MDA-MB-231 cells with monensin (MN), a lysosome-selective ionophore (Grinde, 1983), and simulating the experimental uptake of HCQ in cells after pre-treatment. The model values of cytosolic pH of roughly 7.0 and lysosomal pH of 5.0 worked well with the cell lines used, which are similar to what has been previously reported for MCF7 cytosolic pH (Belhoussine et al., 1999), and MCF7 and MDA-MB-231 lysosomal pH values (Montcourrier et al., 1994). It is noted that the range of the pH values from different literature reports is quite broad, with lysosomal pH values reported around 4.2 for MDA-MB-231 cells (Ndolo et al., 2012), 4.5 for MCF7 and MDA-MB-231 cells (Wang et al., 2019), and 5.1 for MCF7 and MDA-MB-231 cells (Montcourrier et al., 1994). Cytosolic pH exhibited a similar trend from literature, with reported values around 6.9 for MCF7 (Belhoussine et al., 1999), 7.3 for MCF7 (Persi et al., 2018), and 7.4 for MDA-MB-231 and MCF7 (Wang et al., 2012). From the studies using multiple human breast cancer lines, that were also used in this work, the lysosomal and cytosolic pH were not very different between each cell line and so we chose to use fixed values for these parameters across all 4 cell line models. Additional factors that could potentially play a role in cellular uptake and clearance of HCQ, such as acid-phospholipid binding and endo/lysosomal turnover, were not investigated between cell lines.

Evaluation of Model Fit

JPET Fast Forward. Published on November 10, 2020 as DOI: 10.1124/jpet.120.000309
This article has not been copyedited and formatted. The final version may differ from this version.

Model fit versus experimental data was evaluated by comparing the experimental AUC_{0-1hr} or AUC_{0-24hr} to the simulated value for each cell line. Additionally, model accuracy was analyzed by calculating the performance error (PE), median performance error (MPE%) to investigate positive/negative bias, and mean absolute performance error (MAPE%) to determine overall model fit (Gustafsson et al., 1992). These calculations included all timepoints relevant to the parent figure.

Computer Simulation and Software

Intracellular PK model simulation was done in MATLAB, version R2020a (Mathworks; Natick, MA) and the intracellular compartmental system was solved using the ode45 package. Image selection was done in Python, version 3.7.6, using sewar and tqdm packages. Image analysis was done in ImageJ, version 1.52p using methods described above.

Results

Whole Cell Uptake of HCQ is Proportional to Basal Lysosomal Volume Fraction

The *in vitro* PK of HCQ was assessed in 4 human breast cancer cell lines (hBC), MDA-MB-231, MDA-MB-468, T47D, and MCF7 by collecting total cell homogenate at 1, 5, 15, 30, 60, 240, and 1440 minutes after incubating with 10µM HCQ. This concentration of HCQ was chosen as it iswithin the upper range of clinically-achievable plasma C_{max} concentrations. HCQ concentration within the whole cell was determined by normalizing total HCQ in the homogenate to the total cell volume in the homogenate outlined in Supplemental Figure 1. We observed different concentration levels of HCQ for each cell line, which mostly followed the ranking of MDA-MB-231 > MDA-MB-468 > T47D > MCF7 (Fig. 1A). For all 4 hBC lines the HCQ total cellular concentrations increased the longer the cell lines were exposed to the drug up to total cellular concentrations peaking between 0.58-2.67mM, which were 58-267x the extracellular concentration of HCQ, and are consistent with steady-state partition coefficients of HCQ

JPET Fast Forward. Published on November 10, 2020 as DOI: 10.1124/jpet.120.000309
This article has not been copyedited and formatted. The final version may differ from this version.

tissue:plasma from previous *in vivo* studies (McChesney et al., 1967; McChesney, 1983; Wei et al., 1995).

As acidic organelles are suggested to account for a majority of cellular distribution of diprotic lipophilic compounds, we investigated the total lysosomal volume fraction of each cell line using microscope imaging methods outlined in Supplemental Fig. 2. We observed lysosomal percent volume of total cellular volume ranging from 0.50 ± 0.19% in MCF7 cells to roughly 3.67 ± 1.09% in MDA-MB-231 cells (Fig. 1B), which followed roughly the same trend as total cellular uptake of HCQ based on $AUC_{0\text{-}24hr}$ (Fig. 1C). Overall, mean total cell uptake concentrations of HCQ showed a significant Pearson correlation with lysosomal volume fraction for timepoints 5, 15, 30, 60, 240, and 1440 minutes (Fig. 1D). The 1 minute timepoint was not significant, likely due to insufficient time for HCQ to diffuse into the lysosomal compartment. Total exposure to HCQ, as calculated by $AUC_{0\text{-}24hr}$, also had a strong correlation (P=0.032, R^2=0.936) with cellular lysosomal volume fraction (Fig. 1E).

Basal Lysosomal PK Model of HCQ Accounts for Uptake by Adjusting Lysosomal Volume Fraction

To further investigate the *in vitro* PK of HCQ in the 4 hBC lines we used a base pharmacokinetic (PK) model of lysosomotropic drug uptake (Trapp et al., 2008; Kornhuber et al., 2010), and modified it to be specific to the 4 cell lines in the study with experimentally determined lysosomal volume fractions. HCQ *in vitro* PK was modeled as a diffusion-based 3-D system where net flux of HCQ across membranes is driven by the permeability of each ionization state, and ionization state (0, 1^+, 2^+) is a function of pH described by the Henderson-Hasselbach activity ratio. The model consisted of 3 compartments representative of *in vitro* settings, which include culture media, cytosol, and lysosomes (Fig. 2A). Trafficking between compartments was driven by net flux. The lysosomal compartment had a dynamic pH (ΔpH)

JPET Fast Forward. Published on November 10, 2020 as DOI: 10.1124/jpet.120.000309
This article has not been copyedited and formatted. The final version may differ from this version.

term that was a function of lysosomal HCQ concentration, as HCQ is suggested to neutralize the acidic lysosomal pH. Model parameters are listed in Supplemental Table 1.

By adjusting the lysosomal volume fractions for each cell line, we simulated the *in vitro* PK experiment of HCQ administered at 10µM for each cell line out to 1 hour (Fig. 2B). For all cell lines except T47D, the experimentally-derived mean lysosomal volume fraction allowed the simulation to capture the mean concentration of HCQ with a strong fit. The simulation was also run using the 95% CI bounds for the experimentally-derived lysosomal volume fractions to investigate variability due to this parameter. The simulation suggested that the system reaches equilibrium around 30 minutes; however, the experimental PK data for all 4 cell lines suggests that HCQ concentrations in the cell continue to increase steadily at 1, 4, and 24 hours (Fig. 2C). Early timepoints were characterized by chemical kinetic equilibrium, where the cellular physiologic parameters are static, followed by later timepoints where the system physiologic parameters are dynamic. The dynamic system is investigated further in later figures. The model fit for each of the cell lines out to 1 hour is characterized by the ratios of simulated/observed AUC (Table 1), as well as measures of predictive performance PE, MAPE%, and MPE% (Supplemental Table 2). Using a previously determined range of 0.5-2.0 as acceptable ratios for AUC of simulated/experimental, the model captured MDA-MB-231, MDA-MB-468, and MCF7 very closely (0.936, 0.995, 0.980). T47D was underpredicted, but still fell within the acceptable range (0.602). In comparing the model performance error (PE), the model underpredicted early timepoints (1, 5 minutes) for all cell lines except MCF7. Timepoints between 15-60 minutes were predicted with good accuracy, aside from T47D. MAPE%, a metric of model accuracy, suggests that the model predicts individual timepoints in MDA-MB cell lines with about 30% error, T47D around 60%, and MCF7 about 6.5%. Overall, the model underpredicts concentrations (MPE%) by 18.4 and 8.6% in the MDA-MB cell lines, although this is biased by early timepoints error, 64% in T47D, and overpredicts by only 1.3% in MCF7. Observations

JPET Fast Forward. Published on November 10, 2020 as DOI: 10.1124/jpet.120.000309
This article has not been copyedited and formatted. The final version may differ from this version.

from these metrics suggest that T47D cell uptake of HCQ may be better explained by the upper CI bound of its lysosomal volume fraction (1.16%), rather than its mean (0.78%). Model metrics also suggest that early timepoints (1, 5 minutes) in MDA-MB cell lines were either underpredicted based on uptake kinetics, or there was time-based experimental error exacerbated by early timepoint sampling.

We also investigated the influence of the pH parameters on total cellular uptake of HCQ in MDA-MB-231 cells. We measured the pH of incubator-conditioned culture media (5% CO2, 37°C) used in the previous experiments at 7.6, and made acidic culture media at an incubator-conditioned pH of 7.0. As stated in the methods section, we opted out of using culture media buffers other than sodium bicarbonate, such as HEPES, as it has been suggested to activate the MiT/TFE pathway which ultimately results in lysosomal biogenesis (Tol et al., 2018). As the model accurately captured MDA-MB-231 cell lines under neutral conditions, they were exposed to 1 or 10µM HCQ in the conditioned culture media for 1 hour, and the resulting decrease in total cellular uptake of HCQ associated with decreasing media pH was quite dramatic. We observed a 6.4-fold decrease in HCQ uptake at the treated concentrations when switching the media pH from 7.6 to 7.0, such that in most cases the 10µM HCQ uptake at pH of 7.0 was nearly equivalent to the 1µM HCQ uptake at pH of 7.6 (Supplemental Figure 3A). The shape of the simulated kinetics uptake curve was not visibly modified by extracellular pH out to the 1 hour timepoint tested (Supplemental Figure 3B). Interestingly, lysosomotropic drug partition into cells and tissues has been suggested to be significantly reduced by acidic extracellular pH (Wojtkowiak et al., 2011), causing a subsequent resistance of cells to growth inhibition by HCQ. We tested the effect of acidic culture media in blunting HCQ growth inhibition in MDA-MB-231 cells and observed an almost complete reduction in growth inhibition (Supplemental Fig. 3C), similar to the trend described by with CQ (Pellegrini et al., 2014). In addition to testing the influence of extracellular pH directly, we also investigated the contribution of lysosome and

JPET Fast Forward. Published on November 10, 2020 as DOI: 10.1124/jpet.120.000309
This article has not been copyedited and formatted. The final version may differ from this version.

cytosol pH gradient indirectly by treating cells with MN prior to HCQ in order to eliminate the gradient. In MDA-MB-231 cells pretreatment with 25µM MN for 30 minutes prior to HCQ caused a reduction in total cellular uptake of HCQ by 93.2% at 1 hour. We simulated this experiment using the model by changing the lysosomal pH to 7.0 and comparing to the model with lysosomal pH of 5.0 (Supplemental Fig 3D). Overall, the model captured the decrease in total cellular uptake well, with simulated MN (+) / MN (-) concentration ratio of 0.078 versus observed MN (+) / MN (-) concentration ratio of 0.068.

HCQ Increases the Size of the Lysosomal Compartment

While the model captures early timepoint *in vitro* PK (<1hr) of HCQ, as well as variabilities in influential model parameters along the pH gradient, it fails to capture later timepoints as the simulation suggests the system reaches equilibrium when the observed concentrations actually continue to gradually increase out to 24 hours (Fig. 2C). Recent reports suggest that many weakly basic lipophilic compounds, including CQ, activate lysosomal biogenesis by activating the transcription factor EB (TFEB) (Lu et al., 2017; Zhitomirsky et al., 2018; Zhao et al., 2020), which ultimately increases the lysosomal volume fraction of treated cells and should allow them to sequester even more drug than their original baseline (Ruzickova et al., 2019). CQ has been observed to activate TFEB and increase lysosomal content of the cell, so we investigated the capability of HCQ to do the same. Treatment of all 4 hBCs with either HCQ for 24 hours or TFEB-activator Torin1 for 16 hours, caused a significant increase in TFEB activity in the nucleus (Fig. 3A), suggesting it is released from the lysosome and translocated to the nucleus after HCQ treatment. In addition, gene microarray data on all 4 cell lines treated with HCQ or vehicle for 24 hours showed a significant enrichment in expression of the TFEB-associated direct targets in lysosomal function (Fig. 3B) as characterized by the Ballabio group (Palmieri et al., 2011). Treatment of all 4 cell lines with HCQ or Torin1 caused an increase in the relative volume of the lysosome compartment. MCF7 cells had the most

JPET Fast Forward. Published on November 10, 2020 as DOI: 10.1124/jpet.120.000309
This article has not been copyedited and formatted. The final version may differ from this version.

visually-distinct increase in lysosomal burden with both drugs (Fig. 3D). Quantitation of the increase in lysosome-positive area per nuclei suggests a relative increase in 1.59 to 14.93-fold (average 5.90-fold) in the cell lines with 24 hour treatment with HCQ, or Torin1 caused a 2.25 to 10.7-fold (average 5.55-fold) (Fig. 3C). This increase in lysosomal burden by HCQ may have some contribution independent of TFEB as well, as CQ has been shown to induce swelling in lysosomes at higher doses, which is visually apparent in images comparing Torin1 increase in lysosomal burden versus HCQ increase in lysosomal burden in MCF7 (Fig. 3D), and the other 3 cell lines (Supplemental Figure 4). To further investigate lysosomal swelling by HCQ we transfected MDA-MB-468, T47D, and MCF7 cells with a GFP baculovirus for lysosomal associated membrane protein 1, LAMP-1, as it more clearly defines the membranes of individual lysosomes, and imaged cells after treatment with 10μM HCQ for 24 hours. MDA-MB-231 cells would not express the virus and were omitted from this experiment. In the 3 cell lines we observed a dramatic increase in size of some lysosomes after HCQ exposure (Supplemental Figure 5).

Dynamic Lysosomal Volume Accounts for Simulation Error

The original model with a static lysosomal volume compartment was able to capture total cell uptake of HCQ out to 1 hour, but significantly underpredicted 4 and 24 hour timepoints. To account for this error, we incorporated lysosomal biogenesis into the model by adding a dynamically-growing lysosomal volume fraction represented by the proposed mechanism outlined in Figure 4. The growing compartment is represented as a linear increase in lysosomal volume fraction as a function of time: $Vf_{lys}(t) = Vf_{lys\_0} \cdot (1+x \cdot t)$. We found that a 1.5 to 3-fold total increase in lysosomal volume fraction by 24 hours in the dynamic lysosomal model accounted for the underprediction of 4 and 24 hour timepoints predicted by the static lysosomal model (Fig 5A). The simulated 1.5-3 fold increase in lysosomal volume fraction over 24 hours of HCQ exposure was within the 95% CI of the experimentally observed increase due to HCQ in the 4

JPET Fast Forward. Published on November 10, 2020 as DOI: 10.1124/jpet.120.000309
This article has not been copyedited and formatted. The final version may differ from this version.

cell lines shown in Figure 3C, except for T47D. As such, for T47D, we tested an increase of 2.5-fold in lysosomal volume starting from the upper bound of the 95% CI (1.155%), which resulted in a better model fit to 24 hours. Incorporation of this time-based linear increase did not significantly affect timepoints before 1 hour (Fig. 5B).

The model fit, as characterized by the ratios of simulated/observed $AUC_{0\text{-}24hr}$, is shown in Table 2, and measures of predictive performance PE, MAPE%, and MPE% are shown in Supplemental Table 3. Overall, the model captured the early timepoints of the cell lines with good performance, as the AUC and ratios were close to 1. PE followed the same trend to the static model for timepoints 0-1hr, with 4-24 hour timepoints being slightly underpredicted for all cell lines except MCF7 and T47D at 24hr. MAPE% suggests the model fits overall timepoints for all cell lines between 7.53-45.21%, and MPE% suggests a slight underprediction bias for the model. Overall, this experimental data and model simulation suggests that HCQ creates a positive feedback-loop within the cell-lysosomal compartment causing it to increase its own distribution within the cell over time.

Torin1 Increases Size of Lysosomal Compartment Which Increases Cell Uptake of HCQ

While HCQ appears to be able to modify its own distribution, we investigated the capability of direct modification of the cell lysosomal volume fraction to increase HCQ uptake capacity. In Figure 4D we observed that Torin1 increased the relative lysosomal burden by 2.25-10.7 fold. In this experiment we repeated the HCQ cell uptake experiments out to 24 hours, but first pretreated cells with Torin1 (+) or (-) for 16 hours prior to administering HCQ. Pretreatment with Torin1 resulted in a mean increase in cellular uptake of HCQ at all timepoints in all cell lines of 1.4-1.6 fold (Figure 6A). To test this in the context of the *in vitro* PK model, we changed the cell line base lysosomal volume fraction at time 0 based on the mean fold increase of lysosomal fraction by Torin1 from Figure 3, and simulated the dynamic lysosome PK model (Figure 6A). The dynamic lysosome PK simulation suggested that this change in initial

JPET Fast Forward. Published on November 10, 2020 as DOI: 10.1124/jpet.120.000309
This article has not been copyedited and formatted. The final version may differ from this version.

lysosome starting fraction accounts for the increased uptake of HCQ in the cells. For the new data set, the MDA-MB-468 T1 (-) uptake data was simulated against the lower CI basal Vf_{lys} (0.835%) and the T47D against the mean starting Vf_{lys} (0.783%) from Figure 1B. In MDA-MB-231 and 468 cells the mean increase of lysosomes by Torin1 accounted for the increased cell uptake of HCQ in the simulation. In T47D and MCF7, the experimental mean increase in lysosomes by Torin1 from Figure 3C was very high, and so the ratio from the lowest replicate was used to show the increase the model would account for. Comparison of observed versus simulated $AUC_{0\text{-}24hr}$ are shown in Table 3. All simulation/experimental ratios except the T47D and MCF7 mean T1 were within the range of 0.5-2.0; however, T47D and MCF7 simulations using the lowest T1/ctrl lysosome ratio from a replicate did fall within this range. Model performance metrics are shown in Supplemental Table 4. The model for each cell line followed similar performance error (PE) trends to the earlier versions of the models. MAPE% for all cell lines suggests that the model fits overall timepoints between 15.48-61.69%, and MPE% suggests an even spread of over and underprediction of the model across the cell lines. Overall, the cell PK model of HCQ supports that steadily-increasing long term whole cell concentrations, as well as the increase in concentration caused by Torin1 pretreatment are linked directly with the increase in size of the lysosomal compartment observed experimentally.

In addition, we ran the same experiment in MDA-MB-231 cells, except pretreated cells with T1, T1 + MN, or MN alone prior to treatment with HCQ for 1 hour. We observed that the ratio of T1/ctrl was not statistically significant from the ratio of MN-T1/ MN-ctrl (1.6), suggesting that this increase in cell uptake of HCQ is due to only the increase in lysosomal volume fraction induced by T1 (Fig. 6C). In MDA-MB-231, model simulation of the T1 (+) vs. T1 (-) scenarios represented an increase in total cellular uptake of HCQ, but also showed that the lysosomal concentrations in both conditions was roughly the same (Fig. 6D). This suggests that even though the quantifiable concentration of HCQ from a PK study, whole cell or tissue homogenate,

JPET Fast Forward. Published on November 10, 2020 as DOI: 10.1124/jpet.120.000309
This article has not been copyedited and formatted. The final version may differ from this version.

may change, the concentration in the lysosome may be the same. This observation could have implications for PK:PD correlations as the lysosome is the target site of HCQ for autophagy-inhibition.

Discussion

Lysosomes have been observed as a drug sink for many lysosomotropic agents, including many prescribed drugs like doxorubicin, vinblastine, imipramine, and a variety of TKIs, like gefitinib (Skoupa et al., 2020), imatinib (Burger et al., 2015), and sunitinib (Ruzickova et al., 2019). In a recent study by Ruzickova et al. the lysosomotropic agent sunitinib was shown to be capable of increasing overall lysosomal sequestration of the TKIs tested, although this effect was insufficient in reducing sensitivity to the TKIs by the hypothesized mechanism of sequestering them away from their mechanistic target sites as the concentrations tested in culture maintained a static extracellular concentration. The *in vitro* PK model of HCQ supports this finding, and would suggest the same observation as the direct increase of lysosomal volume fraction by pretreating with Torin1 (Fig. 6C) barely increases HCQ concentration in the lysosome even though the whole cell concentration is higher. This observation sheds light onto one commonly suggested hypothesis for HCQ growth-inhibition synergism with other lysosomotropic agents in cell culture, which is that HCQ displaces drugs from the lysosome, reducing overall sequestration, and increasing concentration at target sites elsewhere within the cell. This work in conjunction with other recent findings would suggest that under static extracellular concentrations this hypothesized mechanism is unlikely, as an overall reduced cellular uptake of lysosomotropic drugs may be due to displacement by HCQ, but would not result in a subsequent increase in concentration at the drug's mechanistic target. This does not eliminate this hypothesized mechanism *in vivo* though, as extracellular concentrations are not constant.

JPET Fast Forward. Published on November 10, 2020 as DOI: 10.1124/jpet.120.000309
This article has not been copyedited and formatted. The final version may differ from this version.

Many drugs have been shown to activate TFEB *in vitro* in recent publications (Lu et al., 2017; Zhitomirsky et al., 2018; Zhao et al., 2020), most of which are weakly basic lipophilic agents that would be physicochemically characterized as lysosomotropic. If lysosomotropism is a major factor in the PK of these drugs, as it is for HCQ, then the distribution of these drugs might be altered by their effect on the lysosome as we have observed for HCQ. Our findings emphasize care in cell-level PK studies of drugs with weakly-basic lipophilic structures, especially when attempting to correlate concentration with response. This is especially important when using multiple lysosomotropic agents in combination.

Regardless, the possibility of occurrence of this lysosome-altered distribution is supported by *in vitro* studies in other lysosomotropic agents, whether it be through the activation of lysosomal biogenesis or through lysosomal fusion that is independent of biogenesis (Skoupa et al., 2020), but with limited data to suggest it may occur *in vivo*. HCQ is somewhat unique in this context because of its long half-life combined with often prolonged dosing regimens, which means that tissue will be exposed to relatively high concentrations of the drug for an extended duration. Extended duration of exposure to tissues might exacerbate the lysosomotropic effects due to HCQ, that may not necessarily be prevalent with other drugs that are dosed more short term. We are unaware of any long term preclinical PK studies involving HCQ that investigate multiple timepoints aside from the work by McChesney, EW (McChesney, 1983). This study looked at a variety of different tissues in rats that were treated with HCQ 6 days/week for months, with timepoints at 1, 2, 3, and 7 months. The key observation from this study is that HCQ concentrations continually increase up to 3 months, where dosing is discontinued in the first study. In the 7 month study, HCQ only starts to reach tissue steady-state between 3-7 months in lung, eye, and muscle, but continues to gradually increase in concentration for other tissue. This is particularly interesting as the plasma half-life of HCQ in rats has been observed at around 10.6 hours (Moore et al., 2011), suggesting a disconnect between plasma and tissue

JPET Fast Forward. Published on November 10, 2020 as DOI: 10.1124/jpet.120.000309
This article has not been copyedited and formatted. The final version may differ from this version.

steady-state values. The study by Wei et. al. also investigated HCQ dosing in rats, sampled multiple timepoints of blood over the course of 10 weeks, but only sampled tissue at the 10 week mark (Wei et al., 1995). Interestingly, of the 3 dosing regimens applied to both male and female rats (6 conditions total), only the 8mg/kg regimen in male rats appeared to increase in blood concentration after the first timepoint at 3 weeks, but remained steady after that. For the rest of the dosing regimens, HCQ appeared to remain constant which would suggest that steadily increasing tissue concentrations of HCQ would be undetected by the traditional PK sampling of blood in clinical studies. With limited *in vivo* data available, we would speculate that lysosomal biogenesis plays a role in long-term tissue uptake, although this effect would likely be less pronounced due to overall lower HCQ concentrations.

This work has implications in HCQ PK, both *in vitro* and *in vivo*, particularly in the context of the cancer clinical trial in solid tumors by Barnard et al., where there was no correlation between HCQ concentrations in the tumor and plasma (Barnard et al., 2014). Further data is needed to investigate the concentration/time relationship of this effect and possible maximum values of lysosome volume fractions that are achievable *in vitro*. For this study we modeled the lysosomal compartment as increasing linearly with time, although it is more likely that this effect follows a hyperbolic trend – increasing rapidly, and leveling off to eventually reach a pseudo-maximum. It is also likely that this effect is due to overall exposure to HCQ (AUC) rather than time or concentration alone, but to investigate that a significant number of timepoints and concentrations are necessary in conjunction with subsequent PK analysis to maintain a connection between the lysosomal biogenesis mechanism and PK outcome. In addition, a comprehensive PK/PD study connecting increasing tissue concentrations over the long term with an increase in lysosomal volume of tissues is warranted to truly confirm whether this phenomenon is important to consider *in vivo*.

JPET Fast Forward. Published on November 10, 2020 as DOI: 10.1124/jpet.120.000309
This article has not been copyedited and formatted. The final version may differ from this version.

Author Contributions

Participated in Research Design: K.P. Collins, D.L. Gustafson

Conducted Experiments: K.P. Collins, S. Witta

Contributed New Techniques and Information: K.P. Collins, J.W. Coy, Y. Pang

Performed Data Analysis: K.P. Collins

Wrote or Contributed to Writing of the Manuscript: K.P. Collins, D.L. Gustafson

Footnotes

This work was supported by National Cancer Institute [Grant R01CA190170 Therapeutic Targeting of Autophagy-Dependent Cancer] and by Department of Defense CDMRP Breast Cancer Research Program [Grant BC130103P1 Identifying and Targeting Autophagy Dependence to Eliminate Metastatic Breast Cancer].

Declaration of Interests

The authors declare that no conflict of interest exists.

References

Abeywickrama CS, Wijesinghe KJ, Stahelin RV and Pang Y (2019) Lysosome imaging in cancer cells by pyrene-benzothiazolium dyes: An alternative imaging approach for LAMP-1 expression based visualization methods to avoid background interference. *Bioorganic Chemistry* **91**:103144-103144.

Barnard RA, Wittenburg LA, Amaravadi RK, Gustafson DL, Thorburn A and Thamm DH (2014) Phase I clinical trial and pharmacodynamic evaluation of combination hydroxychloroquine and doxorubicin treatment in pet dogs treated for spontaneously occurring lymphoma. *Autophagy* **10**:1415-1425.

Belhoussine R, Morjani H, Sharonov S, Ploton D and Manfait M (1999) Characterization of intracellular pH gradients in human multidrug-resistant tumor cells by means of scanning microspectrofluorometry and dual-emission-ratio probes. *Int J Cancer* **81**:81-89.

Burger H, den Dekker AT, Segeletz S, Boersma AW, de Bruijn P, Debiec-Rychter M, Taguchi T, Sleijfer S, Sparreboom A, Mathijssen RH and Wiemer EA (2015) Lysosomal Sequestration Determines Intracellular Imatinib Levels. *Mol Pharmacol* **88**:477-487.

Duvvuri M and Krise JP (2005) A novel assay reveals that weakly basic model compounds concentrate in lysosomes to an extent greater than pH-partitioning theory would predict. *Molecular Pharmaceutics* **2**:440-448.

Gallagher LE, Radhi OA, Abdullah MO, McCluskey AG, Boyd M and Chan EYW (2017) Lysosomotropism depends on glucose: a chloroquine resistance mechanism. *Cell death & disease* **8**:e3014-e3014.

Grinde B (1983) Effect of Carboxylic Ionophores on Lysosomal Protein-Degradation in Rat Hepatocytes. *Experimental Cell Research* **149**:27-35.

Gustafsson LL, Ebling WF, Osaki E, Harapat S, Stanski DR and Shafer SL (1992) Plasma concentration clamping in the rat using a computer-controlled infusion pump. *Pharm Res* **9**:800-807.

Ishizaki J, Yokogawa K, Ichimura F and Ohkuma S (2000) Uptake of imipramine in rat liver lysosomes in vitro and its inhibition by basic drugs. *The Journal of pharmacology and experimental therapeutics* **294**:1088-1098.

King MA, Ganley IG and Flemington V (2016) Inhibition of cholesterol metabolism underlies synergy between mTOR pathway inhibition and chloroquine in bladder cancer cells. *Oncogene*:1-11.

Kornhuber J, Henkel AW, Groemer TW, Stadtler S, Welzel O, Tripal P, Rotter A, Bleich S and Trapp S (2010) Lipophilic cationic drugs increase the permeability of lysosomal membranes in a cell culture system. *Journal of Cellular Physiology* **224**:152-164.

Lu S, Sung T, Lin N, Abraham RT and Jessen BA (2017) Lysosomal adaptation: How cells respond to lysosomotropic compounds. *PLoS ONE* **12**:1-23.

Maycotte P, Gearheart CM, Barnard R, Maycotte P, Gearheart CM, Barnard R, Aryal S and Levy JMM (2014) STAT3-Mediated Autophagy Dependence Identifies Subtypes of Breast Cancer where Autophagy Inhibition can be Efficacious. *Cancer Research* **74**:2579-2590.

McChesney EW (1983) Animal toxicity and pharmacokinetics of hydroxychloroquine sulfate. *The American Journal of Medicine* **75**:11-18.

McChesney EW, Banks WF and Fabian RJ (1967) Tissue distribution of chloroquine, hydroxychloroquine, and desethylchloroquine in the rat. *Toxicology and applied pharmacology* **10**:501-513.

Montcourrier P, Mangeat PH, Valembois C, Salazar G, Sahuquet A, Duperray C and Rochefort H (1994) Characterization of very acidic phagosomes in breast cancer cells and their association with invasion. *Journal of Cell Science* **107**:2381-2391.

Moore BR, Page-sharp M, Stoney JR, Ilett KF, Jago JD, Batty KT and Al MET (2011) Pharmacokinetics , Pharmacodynamics , and Allometric Scaling of Chloroquine in a Murine Malaria Model . **55**:3899-3907.

Ndolo RA, Luan Y, Duan S, Forrest ML and Krise JP (2012) Lysosomotropic Properties of Weakly Basic Anticancer Agents Promote Cancer Cell Selectivity In Vitro. *PLoS ONE* **7**:1-9.

Palmieri M, Impey S, Kang H, di Ronza A, Pelz C, Sardiello M and Ballabio A (2011) Characterization of the CLEAR network reveals an integrated control of cellular clearance pathways. *Hum Mol Genet* **20**:3852-3866.

Pellegrini P, Strambi A, Zipoli C, Hägg-olofsson M, Buoncervello M, Linder S and Milito AD (2014) Acidic extracellular pH neutralizes the autophagy-inhibiting activity of chloroquine Implications for cancer therapies. *Autophagy* **10**:562-571.

Persi E, Duran-Frigola M, Damaghi M, Roush WR, Aloy P, Cleveland JL, Gillies RJ and Ruppin E (2018) Systems analysis of intracellular pH vulnerabilities for cancer therapy. *Nature Communications* **9**.

Ruzickova E, Skoupa N, Dolezel P, Smith DA and Mlejnek P (2019) The Lysosomal Sequestration of Tyrosine Kinase Inhibitors and Drug Resistance. *Biomolecules* **9**.

Schmitt MV, Lienau P, Fricker G and Reichel A (2019) Quantitation of lysosomal trapping of basic lipophilic compounds using in vitro assays and in silico predictions based on the determination of the full pH profile of the endo-/lysosomal system in rat hepatocytes. *Drug Metabolism and Disposition* **47**:49-57.

Settembre C, Polito VA, Garcia M, Vetrini F, Erdin S, Erdin SU, Huynh T, Medina D, Colella P, Sardiello M and Rubinsztein DC (2013) TFEB Links Autophagy to Lysosomal Biogenesis. *Science* **332**:1429-1433.

Settembre C, Zoncu R, Medina DL, Vetrini F, Erdin S, Erdin S, Huynh T, Ferron M, Karsenty G, Vellard MC, Facchinetti V, Sabatini DM and Ballabio A (2012) A lysosome-to-nucleus signalling mechanism senses and regulates the lysosome via mTOR and TFEB. *EMBO J* **31**:1095-1108.

Skoupa N, Dolezel P and Mlejnek P (2020) Lysosomal Fusion: An Efficient Mechanism Increasing Their Sequestration Capacity for Weak Base Drugs without Apparent Lysosomal Biogenesis. *Biomolecules* **10**:1-37.

Tol MJ, van der Lienden MJC, Gabriel TL, Hagen JJ, Scheij S, Veenendaal T, Klumperman J, Donker-Koopman WE, Verhoeven AJ, Overkleeft H, Aerts JM, Argmann CA and van Eijk M (2018) HEPES activates a MiT/TFE-dependent lysosomal-autophagic gene network in cultured cells: A call for caution. *Autophagy* **14**:437-449.

Towers CG, Fitzwalter BE, Regan D, Goodspeed A, Morgan MJ, Liu CW, Gustafson DL and Thorburn A (2019) Cancer Cells Upregulate NRF2 Signaling to Adapt to Autophagy Inhibition. *Dev Cell* **50**:690-703 e696.

Trapp S, Rosania GR, Horobin RW and Kornhuber J (2008) Quantitative Modeling of Selective Lysosome Targeting for Drug Design. *European Biophysics Journal* **18**:1317-1328.

Wang K, Tu Y, Wan J-B, Chen M and He C (2019) Synergistic anti-breast cancer effect of pulsatilla saponin D and camptothecin through interrupting autophagic–lysosomal function and promoting p62-mediated ubiquitinated protein aggregation. *Carcinogenesis*:1-13.

Wang L, Niu Z, Zhang L, Liu X, Wang X, Li F and Wang Y (2012) Clinicopathological significance of mesothelin expression in invasive breast cancer. *J Int Med Res* **40**:909-916.

Warhurst DC, Steele JCP, Adagu IS, Craig JC and Cullander C (2003) Hydroxychloroquine is much less active than chloroquine against chloroquine-resistant Plasmodium falciparum, in agreement with its physicochemical properties. *Journal of Antimicrobial Chemotherapy* **52**:188-193.

Wei Y, Nygard GA, Ellertson SL and Khalil SKW (1995) Stereoselective Disposition of Hydroxychloroquine and Its Metabolites in Rats. *Chirality* **7**(8);598-604.

Wojtkowiak JW, Verduzco D, Schramm KJ and Gillies RJ (2011) Drug resistance and cellular adaptation to tumor acidic pH microenvironment. *Molecular Pharmaceutics* **8**:2032-2038.

Zhao B, Dierichs L, Gu JN, Trajkovic-Arsic M, Axel Hilger R, Savvatakis K, Vega-Rubin-de-Celis S, Liffers ST, Pena-Llopis S, Behrens D, Hahn S, Siveke JT and Lueong SS (2020) TFEB-mediated lysosomal biogenesis and lysosomal drug sequestration confer resistance to MEK inhibition in pancreatic cancer. *Cell Death Discov* **6**:12.

Zhitomirsky B, Yunaev A, Kreiserman R, Kaplan A, Stark M and Assaraf YG (2018) Lysosomotropic drugs activate TFEB via lysosomal membrane fluidization and consequent inhibition of mTORC1 activity. *Cell Death Dis* **9**:1191.

JPET Fast Forward. Published on November 10, 2020 as DOI: 10.1124/jpet.120.000309
This article has not been copyedited and formatted. The final version may differ from this version.

Figure 1. Whole cell uptake of HCQ is proportional to basal lysosomal volume fraction

The *in vitro* whole cell PK of HCQ was assessed in 4 human breast cancer cell lines (hBC), MDA-MB-231, MDA-MB-468, T47D, and MCF7 at 1, 5, 15, 30, 60, 240, and 1440 minutes after incubating with 10µM HCQ (A). Cell lysosomal volume fraction was calculated as outlined in Supplemental Figure 2 (B). Lysosomal volume fraction closely followed the ranking of $AUC_{0\text{-}24hr}$ of the whole cell PK data (C). Mean whole cell HCQ concentrations at each timepoint, except 1 minute, was significantly correlated with cellular lysosome volume fraction (D). This correlation was also significant when comparing the mean $AUC_{0\text{-}24hr}$ of each cell line to the cellular lysosome volume fraction (E). Applicable data is shown as mean ± sd, and significance is defined as $P < 0.05$.

Figure 2. Basal Lysosome PK Model of HCQ Accounts for Uptake by Adjusting Lysosomal Volume Fraction

To further investigate the *in vitro* PK of HCQ in the 4 hBC lines we used a previously published base model of lysosomotropic drug uptake into cells. The compartmental model is outlined, where compartments considered are culture media, cytosol, and lysosome, with the lysosome contained within the cytosolic compartment (A). Mathematically, the 3 compartments are separate, where HCQ diffuses freely from Media ←→ Cytosol ←→ Lysosomes, and diffusion is represented by a net flux term (ΔJ) that is the sum of permeability of each HCQ ionization state (neutral, 1+, 2+). The lysosomal compartment has a dynamic pH feedback term that was representative of the proposed mechanism of HCQ to increase the pH of the lysosome based on free drug concentration. The model was used to simulate HCQ uptake in each cell line based on lysosomal volume fractions and other parameters in Table 1. The output of the model simulation for each cell line is shown as the observed mean ± 95% CI bounds in conjunction with the simulated mean ± 95% CI bounds of the cellular lysosomal volume fraction (B). The model only considered timepoints out to the first hour, which were labeled as short-term static

JPET Fast Forward. Published on November 10, 2020 as DOI: 10.1124/jpet.120.000309
This article has not been copyedited and formatted. The final version may differ from this version.

equilibrium. In the experimental data it is observed that concentrations continue to increase after 1 hour, which is characterized as the long-term dynamic system (C), and investigated in later figures.

Figure 3. HCQ Increases the Size of the Lysosomal Compartment

We investigated the ability of HCQ to change the size of the lysosomal compartment. TFEB activity in the nucleus was significantly increased in all cell lines treated with 10µM HCQ for 24 hours, and with 250nM Torin1, a molecular TFEB activating agent, for 16 hours (A). Gene set enrichment analysis (GSEA) of all four cell lines treated with 20µM HCQ for 24 hours also caused a significant enrichment of TFEB lysosome targets (B). Fluorescence microscopy imaging of all 4 cell lines with ETP showed a significant increase in lysosome accumulation within all cell lines treated with 10µM HCQ for 24 hours, or 250nM Torin1 for 16 hours (C). Representative images of MCF7 cells imaged with ETP under the treatment conditions are shown in in (D). Zooming in on MCF7 cells treated with HCQ shows a visual increase in lysosomal size in comparison with the Torin1 treatment. To prepare figures for publication the raw image threshold was adjusted to the same upper and lower bounds across the entire image for all images shown.

Figure 4. HCQ increases the size of the lysosome compartment which should increase its whole cell drug uptake

This figure outlines the process by which HCQ increases its volume of distribution within the cell. HCQ is initially added to the cell culture (1), after which it immediately begins to accumulate within the lysosomes of the cells until it reaches chemical equilibrium between 30 to 60 minutes (2). After reaching chemical equilibrium, the lysosomes begin to swell and simultaneously activate TFEB (3). TFEB triggers the formation of new lysosomes, which undergo the same swelling process under static extracellular concentrations of HCQ (4). This

JPET Fast Forward. Published on November 10, 2020 as DOI: 10.1124/jpet.120.000309
This article has not been copyedited and formatted. The final version may differ from this version.

hypothesized mechanism describes the rapid chemical equilibrium of HCQ within the cell, until it starts causing a dynamic increase in the size of the lysosome compartment, ultimately leading to this positive feedback loop where HCQ increases its own cellular volume of distribution.

Figure 5. Dynamic Lysosome Volume Accounts for Simulation Error in Long-Term HCQ Uptake

To investigate HCQ whole cell uptake past 1 hour, we incorporated a growing lysosomal component into the model for all cell lines. Lysosomal growth is represented by a linear increase as a function of time, out to a maximum lysosomal volume of the fold-increase observed with HCQ treatment for each cell line in Figure 3C. The dynamic system model is shown (A) for MDA-MB-231, MDA-MB-468, T47D, and MCF7, respectively. MDA-MB-231 and MDA-MB-468 simulated uptake are shown as the mean increase in experimental lysosomal volume after HCQ treatment, the upper value of the lysosomal volume, and with no growth incorporated. T47D is shown as the mean, upper, and lower increase in lysosomal volume as well as the value we would expect based on the PK data (realistic) and no growth. MCF7 is shown as the mean, upper, lower, and no growth. It should be noted that the time-based increase in lysosomal volume in the dynamic model does not affect earlier timepoints, and thus would not affect model fit versus the static model out to 1 hour (B).

Figure 6. Torin1 Increases Size of Lysosomal Compartment, Increasing Whole Cell Uptake of HCQ

Cell lines were pretreated with Torin1 (T1) using the same concentration and time as in Figure 3. After Torin1 pretreatment HCQ, the PK studies from 1min-24hr were repeated in Torin1 (+) vs. Torin1 (-) cells. Torin1 pretreatment resulted in an average increase of HCQ whole cell concentrations at all timepoints by an average of 1.4 to 1.6-fold. The mathematical PK model of HCQ was tested at basal lysosomal volume fractions versus Torin1-modified starting lysosomal

JPET Fast Forward. Published on November 10, 2020 as DOI: 10.1124/jpet.120.000309
This article has not been copyedited and formatted. The final version may differ from this version.

volume fractions by multiplying the basal lysosomal volume fraction in each cell line by the mean increase by Torin1 treatment from Figure 4D (A). MDA-MB-231 (A, top-left) fit the data well using mean values of Torin1. MDA-MB-468 used the starting lysosomal volume fraction value of the lower 95% CI (0.753%) and mean value of Torin1 increase (A, top-right). T47D used the mean starting Vf_{lys} (0.783%), and was tested against the mean Torin1 increase in lysosomes (10.5x) as well as the lowest observed ratio within the replicates (3x) (A, bottom-left). MCF7 was tested against the mean lysosomal increase by Torin1, and the lowest observed ratio within the replicates (3.8x) (A, bottom-right). To test if the increase in uptake by Torin1 was only due to the increase in lysosomes MDA-MB-231 HCQ uptake was tested at 1 hour with no pretreatment, Torin1 pretreatment, monensin pretreatment, or Torin 1 and monensin pretreatment. No significant change in the ratio between T1/ctrl and MN+T1/MN HCQ uptake was observed (B) with a two-tailed unpaired t test ($p = 0.573$). Comparing the simulated lysosomal concentrations versus the whole cell uptake concentrations in MDA-MB-231 cells with T1 (+) or (-) show a minimal difference in lysosomal concentration in both scenarios (C).

JPET Fast Forward. Published on November 10, 2020 as DOI: 10.1124/jpet.120.000309
This article has not been copyedited and formatted. The final version may differ from this version.

Table 1. Static Model Metrics (AUC)

AUC Summary (0-1hr)	Experimental	Simulated	Ratio
Cell line	Mean	Mean	Mean Sim / Exp
MDA-MB-231	1239	1160	0.936
MDA-MB-468	551	549	0.995
T47D	588	354	0.602
MCF7	276	270	0.980

JPET Fast Forward. Published on November 10, 2020 as DOI: 10.1124/jpet.120.000309
This article has not been copyedited and formatted. The final version may differ from this version.

Table 2. Dynamic Model Metrics (AUC)

AUC Summary (0-24hr)	Experimental	Simulated	
Cell Line	Mean	Mean	Mean Sim / Exp
MDA-MB-231	55660	46753	0.84
MDA-MB-468	26922	22085	0.82
T47D	26340	56178	2.13
T47D (*realistic*)		21198	0.80
MCF7	11553	16823	1.46
MCF7 (*lower*)		10975	0.95

JPET Fast Forward. Published on November 10, 2020 as DOI: 10.1124/jpet.120.000309
This article has not been copyedited and formatted. The final version may differ from this version.

Table 3. Torin1 Dynamic Model Metrics (AUC)

AUC Summary (0-24hr)	Experimental	Simulated	
Cell Line	Mean	Mean	Mean Sim / Exp
MDA-MB-231 (Ctrl)	56214	46753	0.83
MDA-MB-231 (T1)	104084	99813	0.96
MDA-MB-468 (Ctrl)	18490	13141	0.71
MDA-MB-468 (T1)	29517	30276	1.03
T47D (Ctrl)	17692	15304	0.87
T47D (T1)	28044	119838	4.27
T47D (T1 - *lower*)		39299	1.40
MCF7 (Ctrl)	12849	10284	0.80
MCF7 (T1)	21471	49679	2.31
MCF7 (T1 - *lower*)		30585	1.42

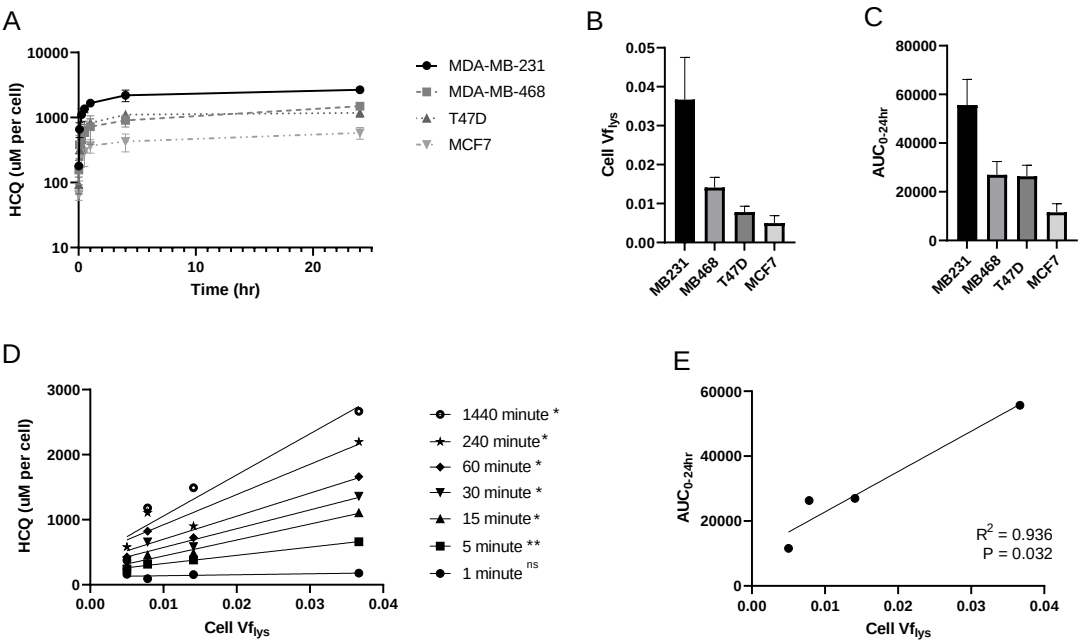
A
HCQ (uM per cell)
Time (hr)
MDA-MB-231
MDA-MB-468
T47D
MCF7
B
Cell Vflys
MB231
MB468
T47D
MCF7
C
AUC0-24hr
MB231
MB468
T47D
MCF7
D
HCQ (uM per cell)
Cell Vflys
1440 minute *
240 minute *
60 minute *
30 minute *
15 minute *
5 minute **
1 minute ns
E
AUC0-24hr
Cell Vflys
R2 = 0.936
P = 0.032

Figure 1

A

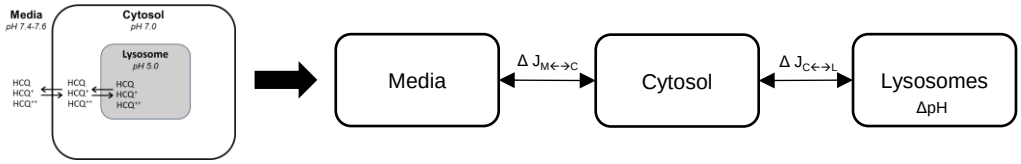
Media
pH 7.4-7.6
Cytosol
pH 7.0
Lysosome
pH 5.0
HCQ
HCQ+
HCQ++
Media
Δ J M←→C
Cytosol
Δ J C←→L
Lysosomes
ΔpH

B

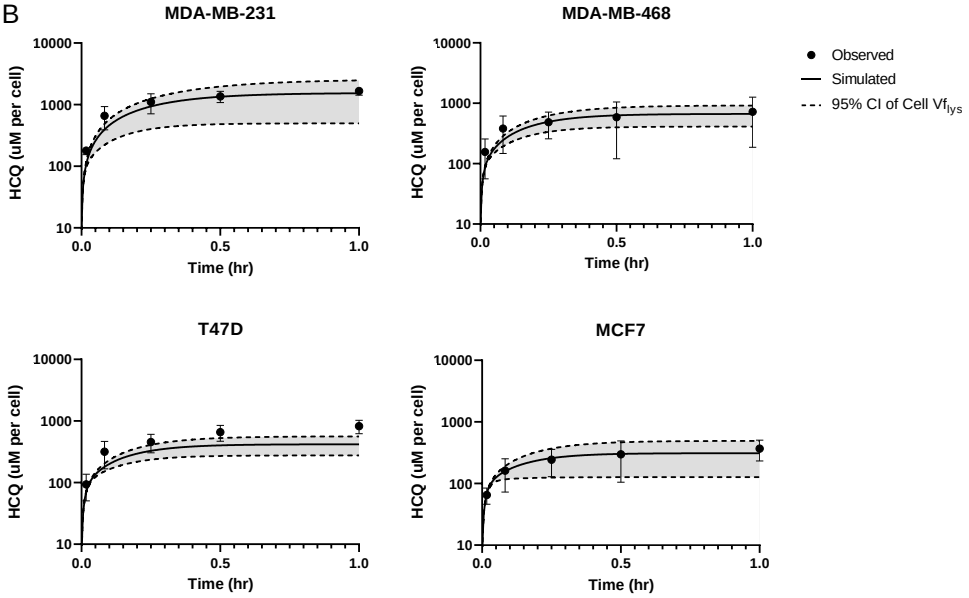
MDA-MB-231
MDA-MB-468
T47D
MCF7
HCQ (uM per cell)
Time (hr)
Observed
Simulated
95% CI of Cell Vf lys

C

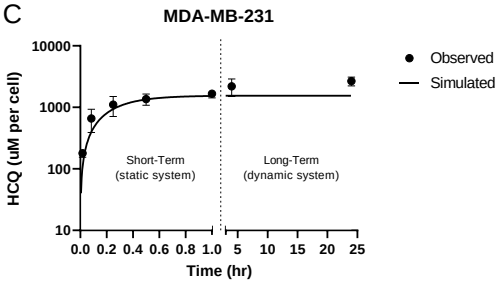
MDA-MB-231
HCQ (uM per cell)
Time (hr)
Short-Term
(static system)
Long-Term
(dynamic system)
Observed
Simulated

Figure 2

JPET Fast Forward. Published on November 10, 2020 as DOI: 10.1124/jpet.120.000309
This article has not been copyedited and formatted. The final version may differ from this version.

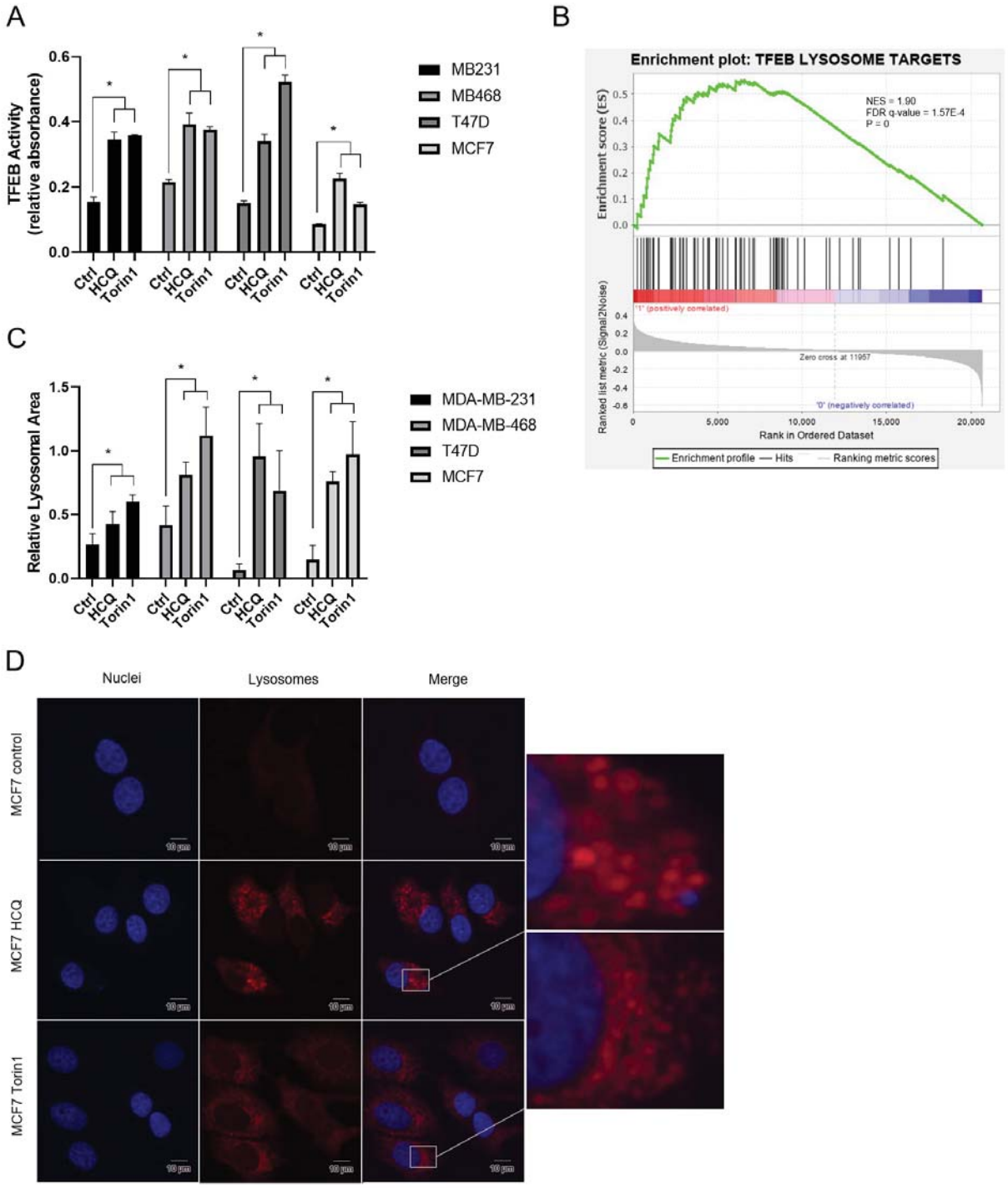

Figure 3

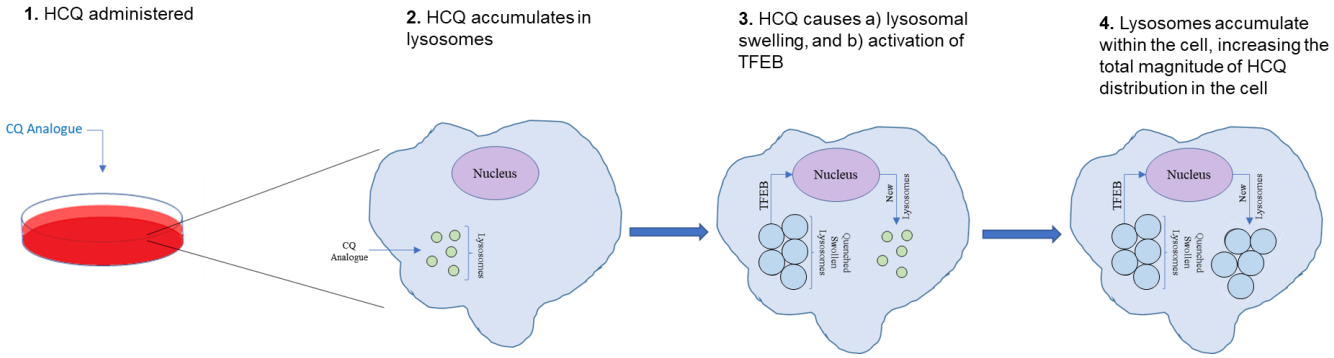
1. HCQ administered
2. HCQ accumulates in lysosomes
3. HCQ causes a) lysosomal swelling, and b) activation of TFEB
4. Lysosomes accumulate within the cell, increasing the total magnitude of HCQ distribution in the cell
CQ Analogue
Nucleus
CQ Analogue
Lysosomes
Nucleus
TFEB
Quenched Swollen Lysosomes
New Lysosomes
Nucleus
TFEB
Quenched Swollen Lysosomes
New Lysosomes

Figure 4

A

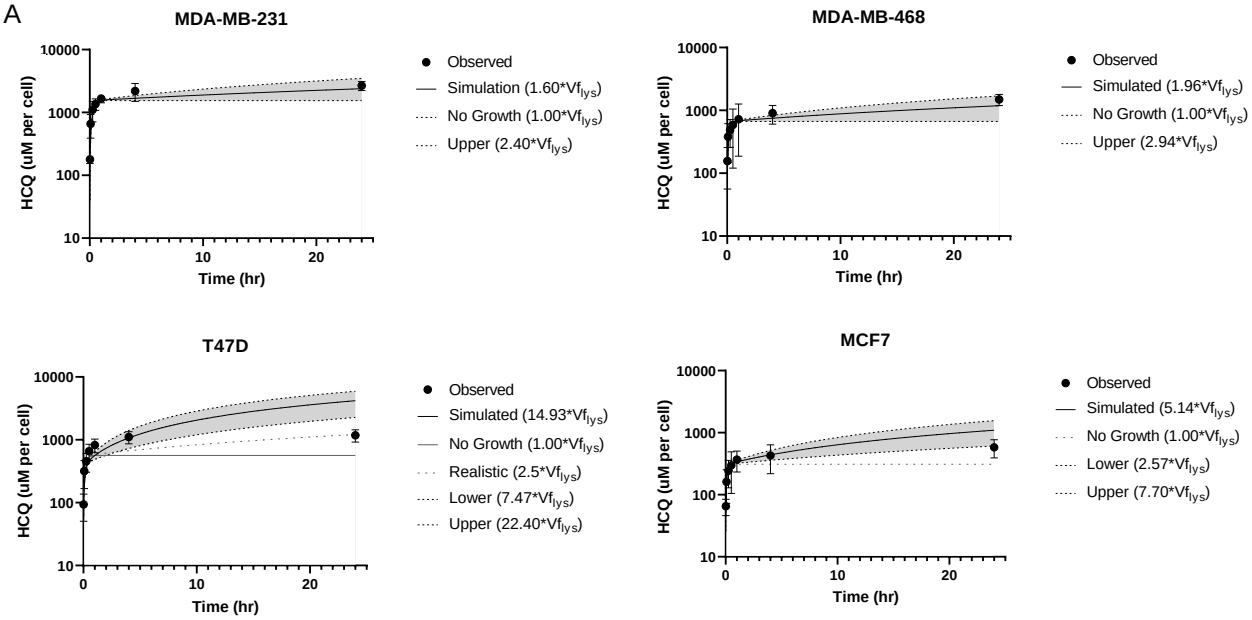
MDA-MB-231
HCQ (uM per cell)
Time (hr)
Observed
Simulation (1.60*Vf$_{lys}$)
No Growth (1.00*Vf$_{lys}$)
Upper (2.40*Vf$_{lys}$)
MDA-MB-468
Observed
Simulated (1.96*Vf$_{lys}$)
No Growth (1.00*Vf$_{lys}$)
Upper (2.94*Vf$_{lys}$)
T47D
Observed
Simulated (14.93*Vf$_{lys}$)
No Growth (1.00*Vf$_{lys}$)
Realistic (2.5*Vf$_{lys}$)
Lower (7.47*Vf$_{lys}$)
Upper (22.40*Vf$_{lys}$)
MCF7
Observed
Simulated (5.14*Vf$_{lys}$)
No Growth (1.00*Vf$_{lys}$)
Lower (2.57*Vf$_{lys}$)
Upper (7.70*Vf$_{lys}$)

B

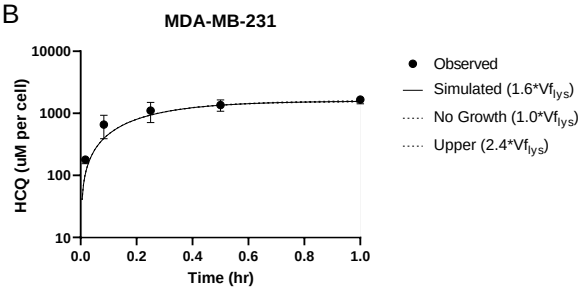
MDA-MB-231
HCQ (uM per cell)
Time (hr)
Observed
Simulated (1.6*Vf$_{lys}$)
No Growth (1.0*Vf$_{lys}$)
Upper (2.4*Vf$_{lys}$)

Figure 5

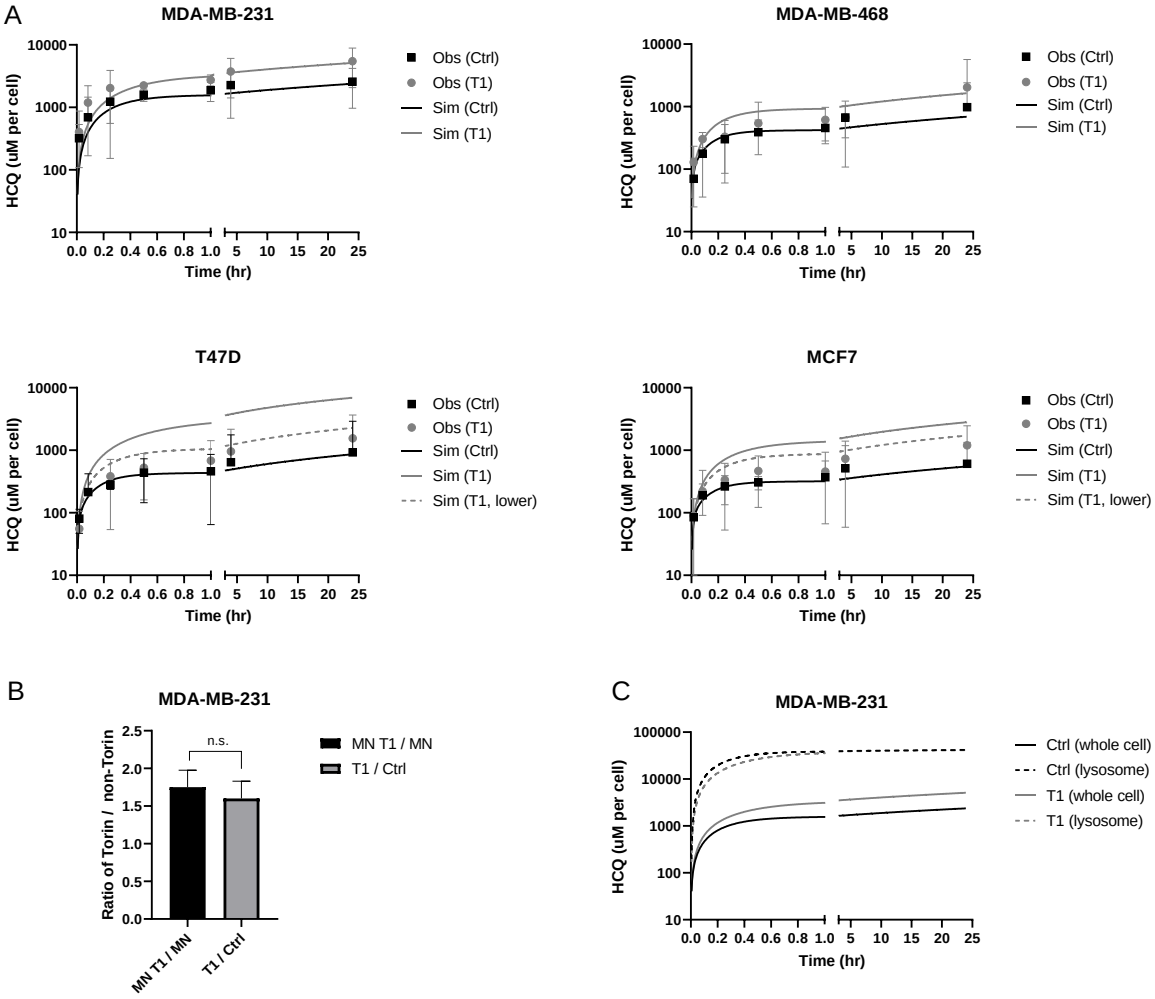
A
MDA-MB-231
MDA-MB-468
T47D
MCF7
HCQ (uM per cell)
Time (hr)
Obs (Ctrl)
Obs (T1)
Sim (Ctrl)
Sim (T1)
Sim (T1, lower)
B
MDA-MB-231
Ratio of Torin / non-Torin
n.s.
MN T1 / MN
T1 / Ctrl
C
MDA-MB-231
HCQ (uM per cell)
Time (hr)
Ctrl (whole cell)
Ctrl (lysosome)
T1 (whole cell)
T1 (lysosome)

Figure 6